Title

Ultrashort Time to Echo Magnetic Resonance Evaluation of Calcium Pyrophosphate Crystal Deposition in Human Menisci

Journal

Investigative Radiology, Publish Ahead of Print(&NA;)

ISSN

0020-9996

Authors

Finkenstaedt, Tim
Biswas, Reni
Abeydeera, Nirusha A
et al.

Publication Date

2019-06-01

DOI

10.1097/rli.0000000000000547

Peer reviewed

HHS Public Access

Author manuscript

Invest Radiol. Author manuscript; available in PMC 2020 June 01.

Published in final edited form as:

Invest Radiol. 2019 June ; 54(6): 349–355. doi:10.1097/RLI.0000000000000547.

Ultrashort Time to Echo (UTE) MR Evaluation of Calcium Pyrophosphate Crystal Deposition (CPPD) in Human Menisci

Tim Finkenstaedt, MD[1,2], **Reni Biswas, BS**[1,3], **Nirusha A Abeydeera, BS**[1,3], **Palanan Siriwananrangsun, MD**[1,4], **Robert Healey**[5], **Sheronda Statum, MS, MBA**[1,3], **Won C. Bae, PhD**[1,3], and **Christine B. Chung, MD**[1,3]

[1.]Department of Radiology, University of California, San Diego, La Jolla, CA [2.]Institute of Diagnostic and Interventional Radiology, University Hospital Zurich, University of Zurich, Switzerland [3.]Department of Radiology, VA San Diego Healthcare System, San Diego, CA [4.]Department of Radiology, Siriraj Hospital, Bangkok, Thailand [5.]Department of Orthopedic Surgery, University of California, San Diego, La Jolla, CA

Abstract

OBJECTIVES: In human menisci, investigate whether calcium pyrophosphate crystal deposition (CPPD) affects biomechanical and quantitative MR properties, and their zonal distribution.

MATERIALS AND METHODS: From nine cadaveric knees, sectioned triangular meniscus pieces were harvested. Samples were classified into “Normal” or “CPPD” groups based upon visual inspection. Micro-CT scan verified CPPD. Using MRI, ultrashort echo time (UTE) T2* and spin echo (SE) T2, quantitative values in three zones (red, red-white and white) were determined. Using biomechanical test, indentation forces (g) in the same zones were determined. Effects of CPPD and meniscal zone on indentation force and quantitative MR values were compared.

RESULTS: On UTE MR images, CPPD-affected menisci exhibited punctate dark regions, found mostly (92%) in avascular white and red-white zones. Indentation forces were significantly higher for CPPD samples in the red-white (all $p<0.02$) and white (all $p<0.004$) zones but not in the vascular red zone (all $p>0.2$). Similarly, UTE T2* red zone values were similar between both groups (~6.6 ms, $p=0.8$) while in the red-white and white zones, CPPD samples had significantly lower values (~5.1 ms, $p=0.005$ to 0.007). In contrast, SE T2 values showed no difference with CPPD ($p=0.12$ to 0.16). UTE T2*, but not SE T2, correlated significantly with indentation force ($R=-0.29$, $p=0.009$).

CONCLUSIONS: Dark CPP deposits were detectable on UTE images featuring high signal intensity from surrounding meniscal tissue. Preliminary results indicate that CPP deposits were almost exclusively found in the avascular zones. Compared to normal, CPPD menisci featured higher indentation stiffness and lower UTE T2* values in the affected zones.

Corresponding author: Christine B. Chung, MD, Department of Radiology, VA San Diego Healthcare System, 3350 La Jolla Village Dr., MC-114, San Diego, CA 92161, phone: (619) 471-0514, fax: (619) 471-0503, cbchung@ucsd.edu.

Keywords

Meniscus; Calcium Pyrophosphate Deposition Disease; Ultrashort echo time; UTE; Indentation testing

INTRODUCTION

Menisci are crucial for even load distribution in the knee by providing congruent contact surfaces through which approximately 45–85% of the joint load is transmitted (1). The menisci contain 15–25% highly organized collagen fibers accounting primarily for the predominantly short T2 properties resulting in its hypointense signal on standard clinical MRI sequences (2, 3). With ultrashort time to echo (UTE) MR techniques (using TE <1 ms) sufficient MR signal of the short T2 components of the menisci can be acquired before the signal decays (4–6). This physical principle builds the foundation for detection of calcifications in the meniscus, as the meniscal tissue appears bright on the UTE images and provides contrast between it and the low signal calcifications. The basic feasibility of this concept has been shown in an MRI study by Omoumi et al. from 2012 (7) on menisci and by Sharma et al. on internal carotid arteries (8), and, in a broader sense, for radiation-free bone imaging of the shoulder (9) and the spine (10).

Meniscal calcifications can be seen in degenerative disease, trauma or calcium pyrophosphate crystal deposition (CPPD) disease (11, 12). CPPD disease of the knee is a common condition particularly in the elderly population (≈10% are affected in age group ≥ 60yrs) that leads to chondrocalcinosis affecting the fibrocartilaginous menisci as one site of predilection (13). Most commonly, CPPD is asymptomatic but can occasionally present as acute CPPD-associated arthritis and is then known as pseudogout. Controversy exists as to whether chondrocalcinosis of the menisci is a consequence of a systemic procalcifying predisposition (14) that may lead to osteoarthritis (15) or is a result of an osteoarthritic process with secondary crystal deposition (16). Pathological meniscal calcifications, which may alter the biomechanical properties of the knee meniscus, may constitute an important contributory factor to osteoarthritis. There is an abundance of literature related to the biomechanical function of healthy menisci (17) including reference values for the aggregate-, tensile and shearing modulus, (18) as well as biomechanical consequences of meniscal tears (19). To our knowledge there is no literature investigating the biomechanical properties of menisci affected by CPPD. There is also a paucity of studies that has investigated the biomechanical alterations of CPPD-affected articular cartilage (20). Furthermore, there is no systematic literature about the distribution of CPPD with regard to three zones of the meniscus that were defined by several studies as the peripheral vascularized “red zone” and the inner avascular “red-white” and “white” zone (21–23). This knowledge would be useful for basic understanding of CPPD formation in menisci, as well as an important diagnostic consideration for characterization of altered meniscal signal on standard MR imaging (24). Further, the presence of CPPD has implications for the therapeutic algorithm in cases of CPPD-affected knees with meniscal tears to decide between a non-operative approach, meniscectomy or primary meniscal repair (25). Frequently, during the assessment of a knee MRI in daily routine no matching radiograph is

present, and even radiographs do not feature a satisfactory sensitivity for detection of calcium deposits (12, 26).

The objective of this study was to investigate whether CPPD-affected menisci exhibit altered biomechanical properties as well as UTE- and spin echo (SE) T2-derived values compared to normal human menisci and if these values may serve as a surrogate for meniscus stiffness. Furthermore, we sought to determine the zonal distribution of the CPP deposits in cadaveric menisci by using micro computed tomography (micro CT) and high-resolution UTE MR imaging.

MATERIALS AND METHODS

This cadaveric study was exempted from the Institutional Review Board (IRB) approval.

Cadaveric specimens

A total of nine previously frozen cadaveric knees of six different donors from the (*blinded for review*) Anatomical Material Program (three women/ three man; 61.3 ± 16.0 years old, mean ± standard deviation) were used. Knees were thawed, and menisci were excised from the knees and sectioned sagittally, into 5 mm thick triangular anterior and posterior horn pieces. By MR imaging, gross inspection, and micro CT (see the section below), samples with normal appearance were placed into “Normal” group (n=15 pieces), and samples affected with CPPD but otherwise normal appearance were placed into “CPPD” group (n=12). The fraction of the meniscus specimens harvested from the medial and lateral menisci was the same for both groups. The remaining samples (n=19) had tear or severe degeneration or were damaged during dissection and were excluded from the study. None of the included knee cadavers showed signs of a previous surgery. Normal samples came from six knees of four donors (three women, one man; mean 62.3 ± 18.2 years old; body mass index (BMI) 15.9 ± 3.0), while CPPD samples came from three knees of two donors (two men; 59.5 ± 16.2 years old; BMI 23.6 ± 8.1). Meticulous documentation of the dissection procedure by photographs was performed to ensure that the harvesting site of the meniscus pieces was accurately matched with the whole cadaveric knee MR images.

Classification of Normal vs. CPPD-affected menisci

The classification menisci into the categories of “Normal” or “CPPD” groups was made by applying the following steps: (1) We selected cadaveric knees (9 of 10) based on a conventional knee MR protocol (Figure 1A) that showed no clear signs of meniscal tear or degeneration as defined by Nguyen et al. (27) and no higher degrees of knee osteoarthritis (≤ grade 2) as defined by Park et al. (28); (2) the selected knees were dissected to harvest anterior and posterior horn menisci, which were visually inspected (Figure 1D) to classify them into “Normal” (n=15) or “CPPD” (n=12) menisci (19 meniscus samples were removed from the study at this stage); (3) the presence or absence of CPP deposits in the selected menisci was confirmed with micro CT scanning and inspection.

MR Imaging

All the MRIs were performed on a 3-T MR Discovery 750 scanner (GE Healthcare, Milwaukee, WI). Prior to dissection, the whole cadaveric knees were scanned with a dedicated 8-channel knee coil, using a standard clinical knee MRI protocol (Figure 1A) as well as 3D Cones (Figure 1BC), a 3D UTE sequence (29), as detailed in Table 1. The 3D Cones prototype sequence uses a unique k-space sampling trajectory that samples data along conical surfaces in 3D (29) and has proven reliable and consistent in past studies (10, 30, 31).

After dissection, the meniscus specimens were mounted onto a custom-made jig that was placed in a syringe filled with Fomblin perfluoropolyether (Solvay SA, Brussels, Belgium) to reduce susceptibility artifacts. The mounted samples were then scanned (Figure 1E) using a custom 1-inch diameter birdcage coil. Scanning protocol of the meniscus specimen is also summarized in Table 1. Briefly, spin echo (SE) T2 map sequence with 8 echo times (TE) ranging from 10 to 80 ms was used to determine T2 values, and a 3D Cones sequence with 4 TE ranging from 0.05 to 12 ms was used to determine UTE T2* values, of the meniscus samples (32).

Micro CT imaging

Micro CT of the meniscus specimens was performed using a Skyscan 1076 CT scanner (Skyscan, Aartselaar, Belgium) with the following parameters: 1 mm aluminum filter, voxel size of 36 μm, x-ray source voltage of 70 kV, current of 141 μA, exposure time of 100 msec, rotation angle of 0.7 degrees, and 3 frames averaging. Reconstruction (Figure 1F) was performed with NRecon (Skyscan) software.

Meniscus zone classification

The “red zone” of the meniscus was defined according to the study from Hauger et al. as the peripheral meniscus rim that constitutes approximately 15% of the meniscus that is located immediately central to the fatty parameniscal connective tissue (21). The length of the entire meniscus specimen was measured (excluding the fatty parameniscal connective tissue) along its long axis. The peripheral 15% of meniscal tissue was assigned to red zone. The residual inner 85% of the meniscus length was equally divided into two halves that were assigned to the outer “red-white” and the inner “white zone” of the meniscus (dotted lines in Figure 2AB). These dotted lines were drawn perpendicular to the flat tibial side of the meniscus.

Indentation Stiffness Assessment

Indentation stiffness testing was conducted by using a dedicated biomechanical testing machine (MACH-1; Biomomentum, Quebec, Canada), equipped with a uniaxial load cell (precision of 0.01 g, maximum load of 150 g) and a 1-mm diameter plane-ended cylindrical indenter. Meniscus samples were placed into custom mold to hydrate and position the cut surface (furthest from the intercondylar eminence) of the sample orthogonal to the indenter. At each site, indentation protocol consisted of an application of 0.1 mm compression at a velocity of 0.1 mm/s, hold for 1 s, and a release at the same velocity, while recording the force. The peak force was determined from the measured force-time data; a higher force represented a stiffer tissue.

The entire cut surface was tested in a grid-pattern with 1-mm spacing, to create contour color map of indentation force (Figure 2CD) using Matlab (version 2017b; Mathworks, Natick, MA). Furthermore, femoral and tibial articular surfaces were also tested along the middle line of the long axis of each specimen with a 1 mm spacing. To spatially register indentation sites to corresponding quantitative MR values, photographs were taken during indentation testing and overlaid with MR images.

Imaging analysis

Meniscus sample gross morphology, MR images, and micro CT images were reviewed in consensus by two board-certified radiologists (*initials blinded for review* and *initials blinded for review)*, with 8 and 7 years of experience of musculoskeletal radiology, respectively. They determined the sample groups (Normal and CPPD), defined the three meniscal zones (red, red-white and white) on images, and identified CPP deposits in MR and micro CT images.

For quantitative MR evaluation, using MATLAB, region of interest (ROI) was drawn for each meniscal zone to calculate SE T2 and UTE T2* values and to create color maps for visualization (Figure 2EF).

Statistics

For each sample and zone, an average of indentation force, SE T2, and UTE T2* value was determined. Using repeated measure ANOVA, effects of pathology (Normal vs. CPPD) and meniscal zone (repeated factor: red, red-white, white zones) on indentation peak force and quantitative MR values were assessed. Planned comparisons were also made to compare zones pair-wise, and to compare Normal vs. CPPD groups within each zone. Correlation between indentation force (on cut surface) vs. MR values were assessed using Pearson correlation.

RESULTS

The gross appearance, indentation force maps, quantitative UTE T2* MR maps, MR images and micro CT images of normal and CPPD-affected menisci are illustrated in Figure 2. Grossly, normal samples were intact with smooth surfaces (Figure 2A), while CPPD samples were characterized by an abundance of punctate and white calcium deposits (Figure 2B), found in white and red-white zones. Indentation force maps indicated that normal menisci (Figure 2C) had lower indentation force than CPPD-affected regions of the menisci (Figure 2D). UTE T2* maps indicated that, compared to normal (Figure 2E), the CPPD-affected regions (Figure 2F) had generally lower T2* values. In normal samples, we did not find signs of CPP deposits on gross image (Figure 2A), the UTE image (Figure 2G), or micro CT (Figure 2I). Interestingly, in all CPPD-affected samples, the red zone is almost always spared from the CPP-deposits, as evident on the gross image (Figure 2B), the UTE image (Figure 2H), and the micro CT image (Figure 2J).

Indentation Force

As shown in Figure 3, the mean indentation force of the meniscus specimen was significantly higher for CPPD-affected than normal meniscus samples in a zone-dependent manner. This was true of all surfaces tested; the effect of CPPD to increase indentation force values was significant when testing the cut surface (Figure 3A, $p<0.0001$), femoral surface (Figure 3B, $p=0.007$) and tibial surface (Figure 3C, $p=0.003$). The interaction between pathology and meniscal zone was also significant in each case (cut surface $p=0.001$; femoral surface $p=0.04$; tibial surface: $p=0.01$), due to the increased indentation forces in the avascular white (all $p<0.004$) and red-white (all $p<0.02$) zones of CPPD samples relative to the normal samples. In the vascular red zone, there was no significant difference between groups (all $p>0.2$).

Quantitative MR values

UTE T2* values showed similar pathologic and zonal trends as indentation forces: red zone values were similar between groups (Normal: 6.4 ± 1.6 ms, CPPD: 6.6 ± 1.6 ms, $p=0.8$) while the values in the red-white (Normal: 6.4 ± 1.2 ms, CPPD: 5.2 ± 0.9 ms, $p=0.007$) and the white zone (Normal: 6.2 ± 1.0 ms, CPPD: 5.1 ± 0.7 ms, $p=0.005$) were significantly lower in the CPPD samples (Figure 4A). In contrast, SE T2 values showed no significant difference between groups in the red-white and white zone ($p=0.12$ to 0.16, Figure 4B).

Correlation between Indentation Stiffness and Quantitative MR values

There was a significant negative correlation between indentation force vs. UTE T2* when considering all meniscus samples ($R=-0.29$, $p=0.009$, Figure 5A). The correlation was much stronger for the subset of CPPD samples ($R=-0.48$, $p=0.003$), but not for the normal samples ($R=+0.19$, $p=0.2$). The indentation force vs. SE T2 did not show significant correlation for all samples ($R=-0.05$, $p=0.676$; Figure 5B), and showed a significant (but weaker than UTE) negative correlation for the CPPD samples ($R=-0.41$, $p=0.013$).

Micro CT

In 11 of 12 (92%) CPPD-affected specimens, the CPP deposits were exclusively found in the red-white and white zones (i.e., avascular zone), but not in the red zone (Figure 1D-F and Figure 2BHJ). Only in one meniscus specimen CPP deposits could be found scattered in the red zone close to the boundary to the red-white zone. CPP deposits were not found in any of the normal samples.

DISCUSSION

Our results showed that CPP deposits are almost exclusively located in the avascular red-white and white zone but not in the vascular red zone of the human menisci. Accordingly, the avascular zone of CPPD-affected menisci has distinctly stiffer biomechanical properties than the corresponding zone of the normal menisci. Consistent with the distribution of the CPP deposits, UTE T2* values were significantly lower in the red-white and white zones of the CPPD samples compared to those zones of the normal menisci. In contrast, conventional SE T2 values could not distinguish CPPD vs. normal samples. SE T2 and T2* values found in our study are comparable to those previously described (2, 33, 34). Human meniscus has

fairly short T2 values making it appear hypointense on conventional MR sequences (7). Commonly, the presence of CPP deposits further shorten the T2 values of the meniscus, but the change is undetectable using conventional MR sequences due to the lack of contrast between the dark deposits within the dark meniscus tissue. Using a TE of less than 0.1 ms, UTE sequence enables T2* characterization of both normal and CPPD-affected menisci, demonstrating its sensitivity to the disease. In addition, we found a strong negative correlation between the UTE T2* values and meniscus stiffness for all meniscus samples. Therefore, UTE T2* may serve as a suitable indicator of meniscus stiffness in CPPD-affected menisci.

A chicken-or-egg controversy exists whether chondrocalcinosis of the menisci may lead to osteoarthritis or is a result of an osteoarthritic process with secondary crystal deposition (14, 16, 35). Our biomechanical results, in line with past indentation studies on healthy human meniscus (36), provide additional data on zonal variations in normal and CPPD-affected menisci, which have not been described before (18, 37, 38). The zonal variation of meniscus stiffness in CPPD-affected menisci could influence their ability to develop hoop stress aiding to compensate for the vertical compressive load (17). However, further investigation is needed to determine if there is a biomechanical ramification of CPPD, such as increased wear of the articulating cartilage and meniscal surfaces due to the presence of hardened crystals.

Our finding that CPP deposits are almost exclusively located in the avascular zones but not in the vascularized red zone of the human menisci has not been described before in the literature. This might be explained by the hypotheses about the genesis of calcium pyrophosphate crystal depositions in tissues stating that these deposits crystalize in a hypoxic environment (39–41), which is more likely found in the avascular red-white and white zone but not in the vascular red zone of the meniscus. In contrast to meniscus, more extensive research has been performed about cartilage and CPP deposits are believed to occur in cartilage due to a combination of metabolic (e.g., high pyrophosphate concentration and by up-regulation of the ANK protein which is responsive to hypoxia via HIF-1α (41)) and cartilage matrix changes in the presence of adequate calcium concentration (20, 41, 42). However, considering the small number of cadaveric knees affected by CPPD in our study, this finding should be considered preliminary.

Our results indicate the feasibility of CPP detection in the meniscus using the UTE technique, which is suitable for the clinical setting (Figure 1BC). Detection of CPPD in the knee using conventional MRI (43, 44) has been successful in articular cartilage but not accurately in the meniscus (43, 44). In contrast, with addition of UTE sequence, it may be possible to detect CPPD in other short T2 tissues of the knee including the menisci. However, additional studies are needed to optimize UTE MR scanning protocols for CPPD detection, and to translate the technique in vivo.

Our study has further limitations. First, we did not perform a histopathological analysis to prove the presence of CPPD. However, the granular or fluffy patterns of deposits in the meniscus specimen as visible on micro CT were very suggestive of CPP deposits (12, 44). Furthermore, we excluded higher grades of osteoarthritis of the cadaveric knees by applying

the MR knee osteoarthritis assessment defined by Park et al. on the knee MR scans prior to dissection (28). Using this approach secondary crystal deposition other than CPP crystals, e.g., dystrophic calcifications in degenerative joint disease, as the underlying cause for this distinct pattern of deposits in the menisci became highly unlikely. Second, the samples had been previously frozen, and the freeze-thaw cycles may have affected our results. However, the freeze-thaw cycles were kept to a minimum and literature indicates that the quantitative MR and biomechanics are not affected greatly by two freeze-thaw cycles (45, 46). Third, CPPD was found in three knees from two donors only. However, inherently it is not feasible to scrutinize cadaver specimens from the University (*blinded for review*) Anatomical Material Program for presence of CPPD before the purchase. Fourth, several meniscus samples were excluded from the study due to tear, severe degeneration or damage during dissection. In those specimens, the biomechanical properties and the quantitative MR values would have been altered and thereby the comparison between both groups “normal” vs. “CPPD-affected” would have been unreasonable. Fifth, the red zone of the meniscus is difficult to define exactly, using even histology, and this may have been a source of error. Past studies have simply assigned a varying range of 10–33% of the periphery to roughly define the red zone (21–23), and we used 15% criteria as defined by Hauger et al. (21). Finally, for the quantitative MR evaluation, we imaged a single slice through the middle of the sample, 1–2 mm beneath the cut surface. In contrast, indentation testing was performed on the cut surface and whose properties may be slightly different from the tissue being imaged.

In conclusion, preliminary results indicate that CPP deposits were almost exclusively found in the avascular red-white and white zone but not in the vascular red zone of cadaveric menisci. Compared to normal menisci CPPD-affected menisci feature distinctly stiffer mechanical properties and lower UTE T2* values in a negatively correlated manner.

Acknowledgments

Disclosure of potential conflicts of Interest:

The study was funded by grants from VA (I01 CX000625) and NIH NIAMS (R01 AR064321) in support of Prof. CB Chung, and NIH NIAMS (R01 AR066622). Furthermore, this work was supported by grant funding from RSNA Research Fellow Grant (RF1730), Swiss National Science Foundation (P2SKP3_168412) and Swiss Society of Radiology in support of Dr. Finkenstaedt. We disclose any financial support or author involvement with organization(s) with financial interest in the subject matter. Its contents are solely the responsibility of the authors and do not necessarily represent the official views of the National Institutes of Health.

REFERENCES

1. Shrive NG, O’Connor JJ, Goodfellow JW. Load-bearing in the knee joint. Clin Orthop Relat Res. 1978(131):279–87. [PubMed: 657636]
2. Williams A, Qian Y, Golla S, Chu CR. UTE-T2 * mapping detects sub-clinical meniscus injury after anterior cruciate ligament tear. Osteoarthritis Cartilage. 2012;20(6):486–94. [PubMed: 22306000]
3. Friebe B, Richter M, Penzlin S, et al. Assessment of Low-Grade Meniscal and Cartilage Damage of the Knee at 7 T: A Comparison to 3 T Imaging With Arthroscopic Correlation. Invest Radiol. 2018;53(7):390–6. [PubMed: 29521888]
4. Williams A, Qian Y, Bear D, Chu CR. Assessing degeneration of human articular cartilage with ultra-short echo time (UTE) T2* mapping. Osteoarthritis Cartilage. 2010;18(4):539–46. [PubMed: 20170769]

5. Han M, Larson PE, Liu J, Krug R. Depiction of achilles tendon microstructure in vivo using high-resolution 3-dimensional ultrashort echo-time magnetic resonance imaging at 7 T. Invest Radiol. 2014;49(5):339–45. [PubMed: 24500089]
6. Springer F, Martirosian P, Schwenzer NF, et al. Three-dimensional ultrashort echo time imaging of solid polymers on a 3-Tesla whole-body MRI scanner. Invest Radiol. 2008;43(11):802–8. [PubMed: 18923260]
7. Omoumi P, Bae WC, Du J, et al. Meniscal calcifications: morphologic and quantitative evaluation by using 2D inversion-recovery ultrashort echo time and 3D ultrashort echo time 3.0-T MR imaging techniques--feasibility study. Radiology. 2012;264(1):260–8. [PubMed: 22723564]
8. Sharma S, Boujraf S, Bornstedt A, et al. Quantification of calcifications in endarterectomy samples by means of high-resolution ultra-short echo time imaging. Invest Radiol. 2010;45(3):109–13. [PubMed: 20065858]
9. Breighner RE, Endo Y, Konin GP, et al. Technical Developments: Zero Echo Time Imaging of the Shoulder: Enhanced Osseous Detail by Using MR Imaging. Radiology. 2018;286(3):960–6. [PubMed: 29117482]
10. Finkenstaedt T, Siriwanarangsun P, Achar S, et al. Ultrashort Time-to-Echo Magnetic Resonance Imaging at 3 T for the Detection of Spondylolysis in Cadaveric Spines: Comparison With CT. Invest Radiol. 2019;54(1):32–8. [PubMed: 30157099]
11. McCarty DJ, Jr., Hogan JM, Gatter RA, Grossman M. Studies on pathological calcifications in human cartilage. I. Prevalence and types of crystal deposits in the menisci of two hundred fifteen cadavera. J Bone Joint Surg Am. 1966;48(2):309–25. [PubMed: 5932916]
12. Zhang W, Doherty M, Bardin T, et al. European League Against Rheumatism recommendations for calcium pyrophosphate deposition. Part I: terminology and diagnosis. Ann Rheum Dis. 2011;70(4):563–70. [PubMed: 21216817]
13. Rosenthal AK, Ryan LM. Calcium Pyrophosphate Deposition Disease. N Engl J Med. 2016;374(26):2575–84. [PubMed: 27355536]
14. Abhishek A, Doherty S, Maciewicz R, et al. Evidence of a systemic predisposition to chondrocalcinosis and association between chondrocalcinosis and osteoarthritis at distant joints: a cross-sectional study. Arthritis Care Res (Hoboken). 2013;65(7):1052–8. [PubMed: 23335553]
15. Derfus BA, Kurian JB, Butler JJ, et al. The high prevalence of pathologic calcium crystals in pre-operative knees. J Rheumatol. 2002;29(3):570–4. [PubMed: 11908575]
16. Mitsuyama H, Healey RM, Terkeltaub RA, et al. Calcification of human articular knee cartilage is primarily an effect of aging rather than osteoarthritis. Osteoarthritis Cartilage. 2007;15(5):559–65. [PubMed: 17276093]
17. Fox AJ, Bedi A, Rodeo SA. The basic science of human knee menisci: structure, composition, and function. Sports Health. 2012;4(4):340–51. [PubMed: 23016106]
18. Makris EA, Hadidi P, Athanasiou KA. The knee meniscus: structure-function, pathophysiology, current repair techniques, and prospects for regeneration. Biomaterials. 2011;32(30):7411–31. [PubMed: 21764438]
19. Richards DP, Barber FA, Herbert MA. Meniscal tear biomechanics: loads across meniscal tears in human cadaveric knees. Orthopedics. 2008;31(4):347–50. [PubMed: 18453170]
20. Roemhildt ML, Beynnon BD, Gardner-Morse M. Mineralization of articular cartilage in the Sprague-Dawley rat: characterization and mechanical analysis. Osteoarthritis Cartilage. 2012;20(7):796–800. [PubMed: 22531460]
21. Hauger O, Frank LR, Boutin RD, et al. Characterization of the “red zone” of knee meniscus: MR imaging and histologic correlation. Radiology. 2000;217(1):193–200. [PubMed: 11012444]
22. Day B, Mackenzie WG, Shim SS, Leung G. The vascular and nerve supply of the human meniscus. Arthroscopy. 1985;1(1):58–62. [PubMed: 4091911]
23. Arnoczky SP, Warren RF. Microvasculature of the human meniscus. Am J Sports Med. 1982;10(2): 90–5. [PubMed: 7081532]
24. Kaushik S, Erickson JK, Palmer WE, et al. Effect of chondrocalcinosis on the MR imaging of knee menisci. AJR Am J Roentgenol. 2001;177(4):905–9. [PubMed: 11566703]
25. Mordecai SC, Al-Hadithy N, Ware HE, Gupte CM. Treatment of meniscal tears: An evidence based approach. World J Orthop. 2014;5(3):233–41. [PubMed: 25035825]

26. Rosenthal AK. Update in calcium deposition diseases. Curr Opin Rheumatol. 2007;19(2):158–62. [PubMed: 17278931]
27. Nguyen JC, De Smet AA, Graf BK, Rosas HG. MR imaging-based diagnosis and classification of meniscal tears. Radiographics. 2014;34(4):981–99. [PubMed: 25019436]
28. Park HJ, Kim SS, Lee SY, et al. A practical MRI grading system for osteoarthritis of the knee: association with Kellgren-Lawrence radiographic scores. Eur J Radiol. 2013;82(1):112–7. [PubMed: 23107172]
29. Gurney PT, Hargreaves BA, Nishimura DG. Design and analysis of a practical 3D cones trajectory. Magn Reson Med. 2006;55(3):575–82. [PubMed: 16450366]
30. Chen B, Zhao Y, Cheng X, et al. Three-dimensional ultrashort echo time cones (3D UTE-Cones) magnetic resonance imaging of entheses and tendons. Magn Reson Imaging. 2018;49:4–9. [PubMed: 29309823]
31. Kim YJ, Cha JG, Shin YS, et al. 3D Ultrashort TE MRI for Evaluation of Cartilaginous Endplate of Cervical Disk In Vivo: Feasibility and Correlation With Disk Degeneration in T2-Weighted Spin-Echo Sequence. AJR Am J Roentgenol. 2018;210(5):1131–40. [PubMed: 29629793]
32. Andreisek G, Weiger M. T2* mapping of articular cartilage: current status of research and first clinical applications. Invest Radiol. 2014;49(1):57–62. [PubMed: 24056113]
33. Chiang SW, Tsai PH, Chang YC, et al. T2 values of posterior horns of knee menisci in asymptomatic subjects. PLoS One. 2013;8(3):e59769. [PubMed: 23555775]
34. Tsai PH, Lee HS, Siow TY, et al. Sequential change in T2* values of cartilage, meniscus, and subchondral bone marrow in a rat model of knee osteoarthritis. PLoS One. 2013;8(10):e76658. [PubMed: 24204653]
35. Fuerst M, Bertrand J, Lammers L, et al. Calcification of articular cartilage in human osteoarthritis. Arthritis Rheum. 2009;60(9):2694–703. [PubMed: 19714647]
36. Choi JY, Biswas R, Bae WC, et al. Thickness of the Meniscal Lamellar Layer: Correlation with Indentation Stiffness and Comparison of Normal and Abnormally Thick Layers by Using Multiparametric Ultrashort Echo Time MR Imaging. Radiology. 2016;280(1):161–8. [PubMed: 26829523]
37. Baro VJ, Bonnevie ED, Lai X, et al. Functional characterization of normal and degraded bovine meniscus: rate-dependent indentation and friction studies. Bone. 2012;51(2):232–40. [PubMed: 22449445]
38. Moyer JT, Priest R, Bouman T, et al. Indentation properties and glycosaminoglycan content of human menisci in the deep zone. Acta Biomater. 2013;9(5):6624–9. [PubMed: 23321302]
39. Hirose J, Ryan LM, Masuda I. Up-regulated expression of cartilage intermediate-layer protein and ANK in articular hyaline cartilage from patients with calcium pyrophosphate dihydrate crystal deposition disease. Arthritis Rheum. 2002;46(12):3218–29. [PubMed: 12483726]
40. Johnson K, Terkeltaub R. Upregulated ank expression in osteoarthritis can promote both chondrocyte MMP-13 expression and calcification via chondrocyte extracellular PPi excess. Osteoarthritis Cartilage. 2004;12(4):321–35. [PubMed: 15023384]
41. Zaka R, Dion AS, Kusnierz A, et al. Oxygen tension regulates the expression of ANK (progressive ankylosis) in an HIF-1-dependent manner in growth plate chondrocytes. J Bone Miner Res. 2009;24(11):1869–78. [PubMed: 19419319]
42. Zaka R, Williams CJ. Role of the progressive ankylosis gene in cartilage mineralization. Curr Opin Rheumatol. 2006;18(2):181–6. [PubMed: 16462526]
43. Miksanek J, Rosenthal AK. Imaging of calcium pyrophosphate deposition disease. Curr Rheumatol Rep. 2015;17(3):20. [PubMed: 25761927]
44. Abreu M, Johnson K, Chung CB, et al. Calcification in calcium pyrophosphate dihydrate (CPPD) crystalline deposits in the knee: anatomic, radiographic, MR imaging, and histologic study in cadavers. Skeletal Radiol. 2004;33(7):392–8. [PubMed: 15138720]
45. Lewis PB, Williams JM, Hallab N, et al. Multiple freeze-thaw cycled meniscal allograft tissue: A biomechanical, biochemical, and histologic analysis. J Orthop Res. 2008;26(1):49–55. [PubMed: 17676620]

46. Pownder SL, Shah PH, Potter HG, Koff MF. The effect of freeze-thawing on magnetic resonance imaging T2* of freshly harvested bovine patellar tendon. Quant Imaging Med Surg. 2015;5(3): 368–73. [PubMed: 26029639]

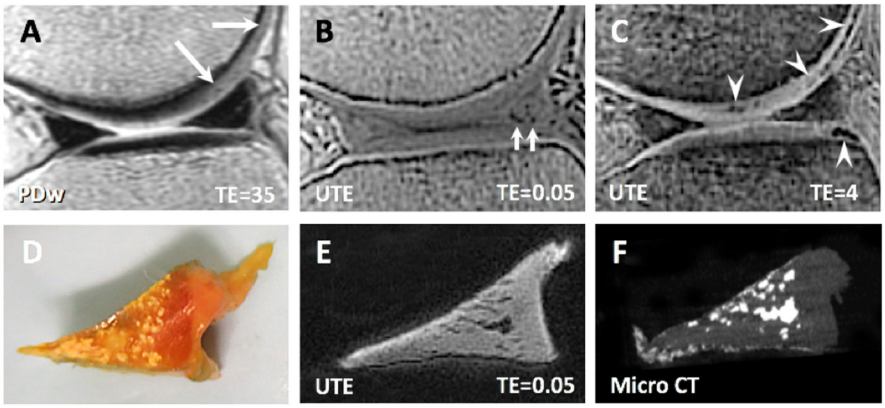

Figure 1.

MR imaging of a knee from a 71-year old male donor (A, B, C) with a scan protocol suitable for the clinical setting and the corresponding sample of the posterior horn of the lateral meniscus (D, E, F). On the proton density weighted image (PDw) at echo time (TE) of 35 ms (A), CPP deposits are not visible within the dark meniscus. In contrast, on the ultrashort echo time (UTE) image using an TE of 0.05 ms (B), sufficient signal is obtained from the short T2 meniscal tissue, provides a good contrast against the dark CPP deposits (short arrows) in the posterior horn meniscus. However, on the UTE image at TE=4 ms (C), the signal of the meniscus has decayed and detection of CPP deposits in the meniscus becomes difficult. After dissection, the same meniscus sample from the posterior horn is shown grossly on the surface (D), and imaged with UTE MR technique (E) as well as with micro CT image (F) on a middle slice. In these images (D-F), localization of CPPD in avascular white and red-white zones is obvious.

Note that on the PD NFS image, a few dark CPP deposits (A, arrows) are vaguely visible within articular cartilage of the femoral condyle, due to the fact that the cartilage has longer T2 components than the meniscus and thus appears with high signal intensity. In comparison, on the UTE image at TE=4 ms, greater number and extent of dark CPP deposits in the femoral and tibial cartilage (C, arrowheads) are seen, with a high contrast.

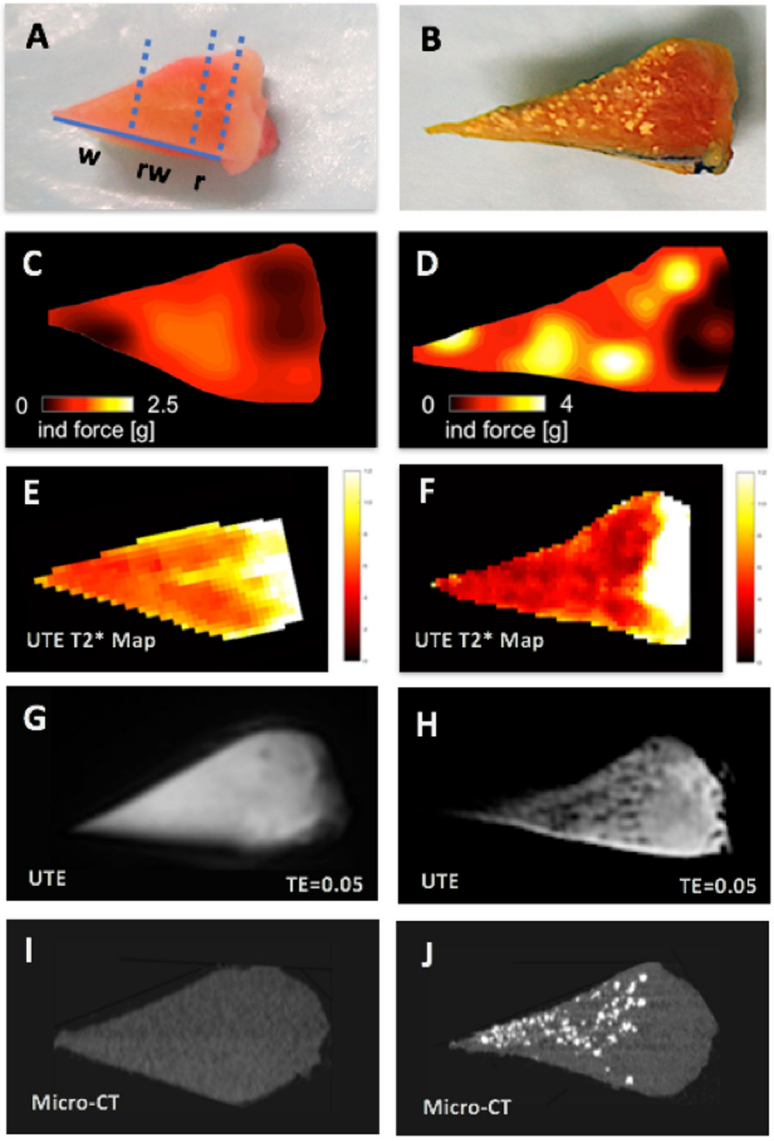

Figure 2.

Gross photographs of menisci belonging to normal (**A**) and CPPD (**B**) groups. Corresponding indentation force maps (**C**, **D**) of the cut surface suggests that compared to normal (**C**), CPPD (**D**) samples have distinctly stiffer biomechanical properties. UTE T2* maps (**E**, **F**) suggest relatively lower values in the CPPD sample (**F**). Note that for the CPPD sample, the red zone is largely spared from CPP-deposits as visible on the gross image (**B**), and have relatively low indentation force (**D**), and relatively high UTE T2* value (**F**) than the white and red-white zones. On UTE MR images (**G**, **H**) with a TE of 0.05 ms, the meniscal tissue appears uniformly bright in normal sample (**G**), or bright with punctate dark CPP deposits in CPPD sample (**H**). These findings were confirmed in micro CT images, showing no CPP deposits in normal sample (**I**), and punctate bright deposits in CPPD sample (**J**).

Abbreviations: r = red zone; rw = red-white zone; w = white zone.

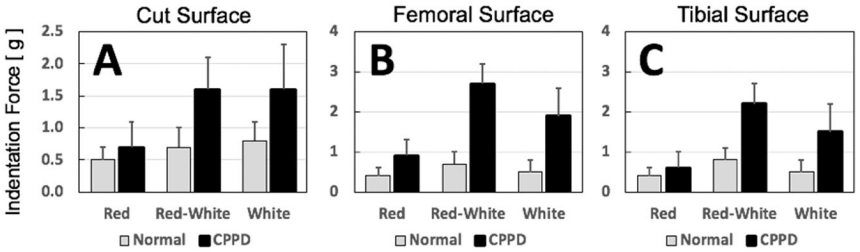

Figure 3.

Comparison of indentation force between Normal vs. CPPD-affected menisci in different zones. CPPD-affected menisci exhibited higher indentation force on the cut surface (**A**), femoral surface (**B**) and tibial surface (**C**) of the menisci than normal menisci. The higher values were found in the red-white and the white zone, but not in the red zone. This is consistent with the distribution of the CPP deposits, which were found mostly in the avascular red-white and white zones. Error bars represent standard deviation.

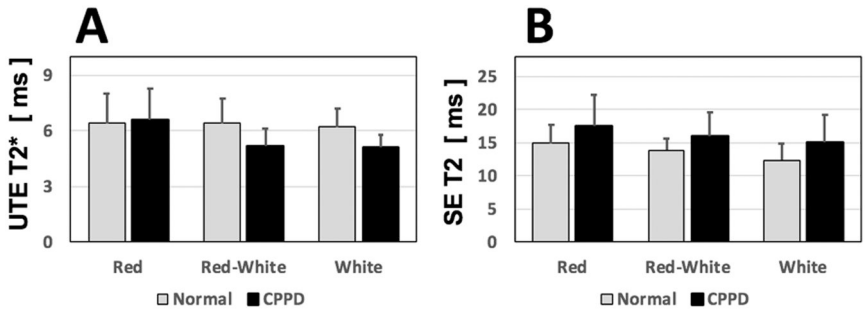

Figure 4.

Comparison of quantitative MR values between Normal vs. CPPD-affected menisci in different zones. CPPD-affected menisci had significantly lower ultrashort echo time (UTE) T2* values (**A**) in the avascular red-white and white zones (each $p<0.01$) but not in the red zone ($p=0.8$), which was mostly spared from the CPP deposits. In contrast, spin echo (SE) T2 values (**B**) showed a tendency towards slightly higher values in the three zones, but this did not reach a statistical significance ($p=0.07$ to 0.16).

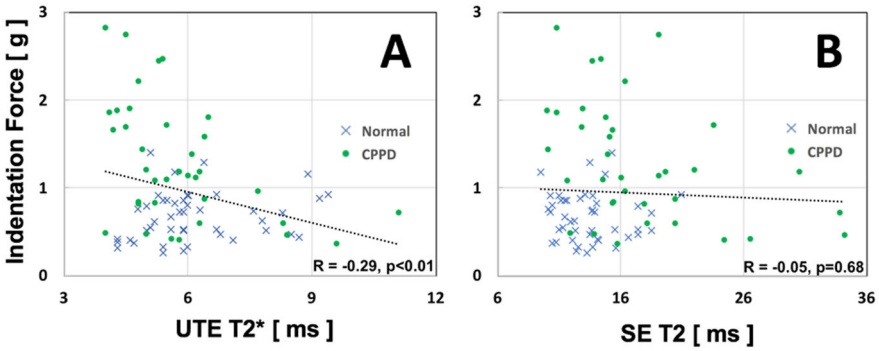

Figure 5.

Correlation of quantitative MR with indentation force values. There was negative correlation between indentation force vs. ultrashort echo time (UTE) T2* values (**A**) for all samples and zones, particularly for the CPPD samples (circle). The indentation force vs. spin echo (SE) T2 values (**B**) showed no significant correlation. The trend lines represent linear trend for all data (normal and CPPD-affected samples combined, and three zones combines).

Table 1.

MR scanning parameters for the whole cadaveric knee and the meniscus specimen scanning. Abbreviations: TR = repetition time; TE = echo time; FOV = field of view; BW = bandwidth; FA = flip angle; PDw = proton density weighted; UTE = ultrashort time-to-echo; SE = Spin-echo.

	Sequence	TR (msec)	TE (msec)	Acquisition Matrix	Slice (mm)	FOV (cm)	BW (±)	FA (°)	Scan time (min)
Whole knee	Sagittal PDw	3900	35	448×224	2	14	36	142	5:36
	3D Cones UTE	13	0.05, 4	320×320	1.7	14	125	10	4:43
Meniscus specimen	SE T2 map	1392	10-80 (8 TEs)	320×256	2	6	21	90	5:59
	3D Cones UTE	13	0.05, 6	402×402	0.2	8	83	10	1:50
	3D Cones UTE map	22	0.05, 4, 8, 12	384×384	2.5	8	83	13	1:39